THE JOURNAL OF PHYSICAL CHEMISTRY C
Cite This: J. Phys. Chem. C 2019, 123, 30059−30066
Article
pubs.acs.org/JPCC

High-Pressure Synthesis of Novel Polyhydrides of Zr and Hf with a Th_4H_{15}-Type Structure

Mikhail A. Kuzovnikov*[,†,‡] and Marek Tkacz[§]

[†]Max Planck Institute for Chemistry, Hahn-Meitner-Weg 1, 55128 Mainz, Germany
[‡]Institute of Solid State Physics RAS, 142432 Chernogolovka, Moscow District, Russia
[§]Institute of Physical Chemistry PAS, Kasprzaka 44/52, 01-224 Warsaw, Poland

Supporting Information

ABSTRACT: The reaction of ZrH_2 and HfH_2 with molecular hydrogen was studied by in situ X-ray diffraction in a diamond anvil cell at room temperature at high pressures of up to 39 GPa. The formation of novel zirconium and hafnium hydrides was observed at 8.2(5) and 12.4(5) GPa, respectively. These new hydrides had the cI16-type structure of a metal lattice, identical to that of Th_4H_{15}, and the compositions of new hydrides were estimated to be Zr_4H_{15} and Hf_4H_{15} on the basis of their lattice volumes. The decomposition of these hydrides back into ZrH_2 and HfH_2 during decompression was observed at 3.5(3) and 3(1) GPa, respectively. Electrical resistance measurements indicated that Hf_4H_{15} is a superconductor with $T_c \approx 4.5$ K at 23 GPa.

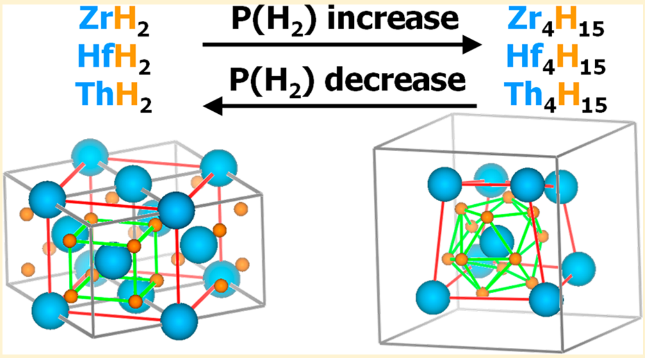

INTRODUCTION

Metal hydrides are important materials for hydrogen and energy storage applications. The discovery of superconductivity in the sulfur−hydrogen system under high pressure at a temperature of 200 K[1] was followed by the renewal of interest in the fundamental properties of hydrides, which are dominated by their metallic character and high-frequency vibrations of hydrogen atoms.

Until recently, no hydrides of transition metals in groups IV−XII were known with composition H/Me > 2. The strong dependence of the Gibbs free energy of molecular hydrogen on pressure makes the latter an ideal tool for the synthesis of new hydrogen-rich compounds. Thanks to the development of the diamond anvil cell (DAC) technique, hydrogen pressures on the order of 100 GPa became routinely available in many laboratories, which allowed the synthesis of a series of new unexpected transition-metal polyhydrides, such as $TaH_{2.2}$,[2] TaH_3,[3] $NbH_{2.5}$ and NbH_3,[4] IrH_3,[5] FeH_3,[6] and even FeH_5.[7]

At the same time, the trihydrides of all rare-earth metals, counting Y and Sc, form under relatively mild conditions and are well known. Recently it was demonstrated that at the hydrogen pressure above 100 GPa lanthanum forms a series of superhydrides with H/La presumably up to 10[8] or 12.[9] Fcc-LaH_{10} was proven to have exceptional superconductive properties, with the claimed T_c value to be above 260 K[10] or about 250 K in later, more accurate measurements.[9] Other rare earth metals, such as cerium, praseodymium, and neodymium, form superhydrides with presumable compositions of up to CeH_9,[11,12] PrH_9,[13,14] and NdH_9,[15] respectively. Recently, yttrium was found to form hydrides with compositions of up to YH_6[16] and YH_9,[17] which are superconducting with T_c values of 224 and 243 K, respectively.

The chemical properties of actinides are somewhat intermediate between those of rare earth and transition metals. Among the actinides, the interaction with hydrogen is best studied for Th and U. Two thorium hydrides are known under ambient conditions: ThH_2, structurally identical to the dihydrides of group IV transition metals Ti, Zr, and Hf; and Th_4H_{15}, whose composition, crystal structure, and properties until now were unique among all hydrides. Despite Th_4H_{15} being the first hydride in which superconductivity was discovered,[18] the absence of the isotopic effect in T_c is still puzzling. The crystal structure of the Th sublattice in Th_4H_{15} is of the cI16 type,[19] which can be described as a distorted 2 × 2 × 2 supercell of the bcc lattice. Within the $I\bar{4}3d$ space group, the thorium atoms in Th_4H_{15} occupy the 16c (x, x, x) positions with positional parameter $x = 0.042$ (with the undistorted bcc lattice corresponding to $x = 0$). The hydrogen atom localization in the unit cell and stoichiometry justification were first given on the basis of the crystal chemistry considerations alone[19] and then were confirmed by neutron diffraction on a deuterated sample.[20] The cI16-type crystal structure is rare, and among the elements, it was observed only in lithium,[21] sodium,[22] and phosphorus[23] under high pressures. Recently, novel niobium and tantalum hydrides with cI16-type crystal structures of the metal sublattice and tentative

Received: August 19, 2019
Revised: November 14, 2019
Published: November 25, 2019

DOI: 10.1021/acs.jpcc.9b07918

compositions NbH_3[4] and TaH_3[3] were discovered under high hydrogen pressures. Apart from the composition difference with Th_4H_{15}, these new trihydrides are characterized by less distortion with $x(NbH_3) = 0.026$ and $x(TaH_3) = 0.033$.

In the U–H system, only two hydrides were known until recently: α-UH_3 with a bcc metal sublattice and β-UH_3 with an A15-type metal sublattice. A series of new uranium[24] and thorium[25] polyhydrides were recently discovered under high pressure, with claimed H/U and H/Th contents of up to 9 and 10, respectively.

Group IV transition metals Ti, Zr, and Hf form a series of hydrides with a composition of up to H/Me = 2. At room temperature and below, these metals form the following phases with hydrogen: an α phase, which is a primary hydrogen solution in an hcp metal lattice; a γ phase, which is a stoichiometric monohydride with a distorted fcc metal lattice and hydrogen ordered at the tetrahedral interstitials; a δ phase, which is a substoichometric (H/Me ≈ 1.6) dihydride with a CaF_2-type structure; and a nearly stoichiometric ε-phase dihydride, which has a tetragonally distorted CaF_2-type structure,[26] also known as the ThH_2-type structure. The stability of the γ phase was debated for a long time, but eventually it was demonstrated that the γ phase is stable in the Ti–H and Zr–H systems.[27]

Recent ab initio calculations for the Zr–H system predicted that ZrH_3 with an hcp metal lattice should be stable at hydrogen pressure above 0[28] or 3 GPa.[29] However, other calculations suggested that ZrH_3 should have a bcc metal lattice and should be stable at hydrogen pressures of between 0 and 130[30] or 110 GPa,[31] with higher hydrides, such as ZrH_4[31] and ZrH_6,[30] being stable at higher pressures. For the Hf–H system, the formation of hcp-HfH_3 was predicted above about 3 GPa.[29]

In this work, we report on the study of zirconium and hafnium under high hydrogen pressure of up to 39 GPa. Instead of the predicted trihydrides, we observe the formation of novel Zr_4H_{15} and Hf_4H_{15} polyhydrides with crystal structures of the Th_4H_{15} type. Electrical resistance measurements revealed a superconductivity in Hf_4H_{15} with $T_c \approx 4.5$ K at 23 GPa.

EXPERIMENTAL DETAILS

Starting Materials. As starting materials, we used iodide-processed zirconium and hafnium. Zirconium was additionally zone-melted at ISSP RAS. Impurity content analysis demonstrated that the metal was 99.95% pure (purity includes hafnium content), with the major impurities being Cu (200 ppm) and Fe (138 ppm). The hafnium purity was 99.5% (including zirconium).

To obtain ε-phase dihydrides, we hydrogenated a zirconium bar and hafnium chips in a Sieverts-type apparatus at $P(H_2) \approx$ 120 bar and $T = 450$ °C for 24 h. The samples were handled in an Ar glovebox with a residual oxygen and water content of less than 1 ppm. The composition of the samples was $ZrH_{2.03(2)}$ and $HfH_{2.06(5)}$ as measured by weighing. The XRD patterns of the dihydrides, measured with an Empyrean diffractometer under ambient conditions, are shown at Figure 1.

In Situ X-ray Diffraction Studies. There were three Zr–H runs (nos. 1–3) and two Hf–H runs (nos. 4 and 5) in which in situ energy-dispersive X-ray diffraction (EDXRD) was studied. For the DAC experiments, we selected metal pieces, which were free from the thin black oxide layer that formed after hydrogenation at the original metal surfaces. The

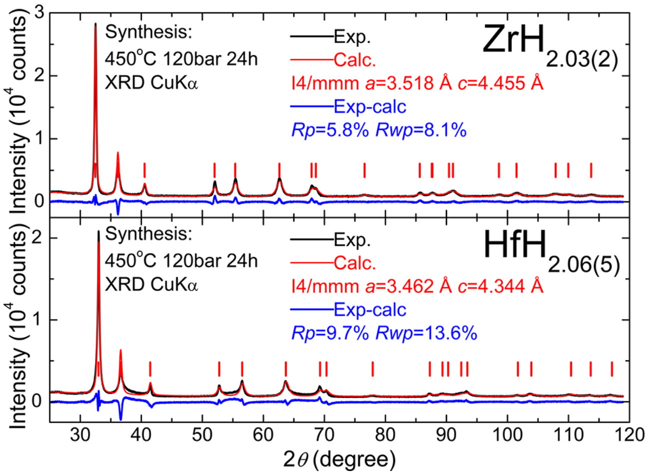

Figure 1. XRD patterns of the initial ZrH_2 (top) and HfH_2 (bottom) samples hydrogenated at 120 bar. Ambient pressure, room temperature, and Cu Kα radiation. The black curves stand for the experimental data, the red curves show the Rietveld fits, and the blue curves are the fit residuals. The rather large residual R factors are mostly due to the anisotropic peak broadening, probably caused by the composition inhomogeneity throughout the samples.

dihydrides were very brittle, and we crushed them in an agate mortar before loading the powder in a DAC. Diamonds of the modified brilliant cut type with flat culets of about 400 μm diameter were used in the DAC. The rhenium gasket was preindented at a pressure of ~15 GPa to ~50 μm thickness, and a hole ~200 μm in diameter was made by a laser. After the desired sample was loaded into the DAC in the Ar box, the DAC was clamped, extracted from the box, placed in the hydrogen loading system, and reopened so that the hydrogen could fill the hole with the sample in the gasket at room temperature and a pressure of ~0.3 GPa. The DAC cell, the hydrogen loading system, and the EDXRD setup used in runs 1–5 are described elsewhere.[32]

Unless otherwise stated, hydrogen was always present in excess, as monitored by Raman spectroscopy, and it served both as a reagent and as a pressure-transmitting medium. The pressure was determined to an accuracy of ±0.3 GPa with the ruby fluorescence method.[33] After each pressure change, the samples were equilibrated for about 1 h and the X-ray powder diffraction pattern was then accumulated during approximately 1 day of exposure. The diffraction was measured using polychromatic radiation from a conventional tungsten target tube collimated down to about 100 μm.[34] The cathode voltage of the tube was −50 kV, and the tube current was 20 mA. The 2θ X-ray scattering angle was set at about 10–12° and calibrated at the beginning of each run using a diffraction pattern of the initial dihydrides at ambient pressure. The energy scale was calibrated independently before and after each pattern was taken by measuring the positions of the Cu Kα, In Kα and La Kβ X-ray fluorescence lines from separate standards and assuming a linear relationship between the channel number of the multichannel analyzer and the photon energy. Additional control of energy calibration in runs 1–3 was provided by using Zr Kα and Zr Kβ fluorescence lines as an internal standard. The resolution of the setup was $\Delta d/d \approx 5\%$. The lattice parameters of the synthesized phases were obtained by the le Bail refinement of experimental energy-dispersive XRD patterns normalized to a constant background level. Runs 1–5 were conducted at room temperature.

Resistance Measurements. In one Hf−H run with a separate DAC cell (no. 6), we studied the electrical resistance. Diamonds with a culet diameter of ∼30 μm beveled at 8° to about ∼200 μm were used. The pressure was determined from the edge of the diamond Raman line[35] and from the position of the H_2 vibron.[36] To make the measuring electrodes in the van der Pauw four-probe geometry, two conductive layers were sputtered onto the surface of one of the diamond anvils in an X-shaped pattern through a mask with a Gatan 682 PECS. We sputtered an ∼50 nm tungsten layer to ensure strong adhesion to the diamond surface and an ∼50 nm gold layer. At this stage, the total resistance of the current leads was about 50 Ω/electrode, as measured by a two-probe technique. The final shape of the electrodes was cut from the X-shaped pattern with a focused beam of Xe ions (FERA3 TESCAN) so that the distance between the opposite electrodes was about 3.5 μm. A stainless steel gasket support was electrically insulated from the electrodes by the layers of cBN and CaF_2 mixtures with low-viscosity epoxy. The central part of the insulating gasket was made of a 4:1 (by weight) mixture of MgO with low-viscosity epoxy. A hole with a diameter of 36 μm was drilled in a gasket of about 7 μm thickness with a 266 nm pulsed laser (Tempest 20). The details of the measurement technique and sample- and gas-loading procedure are given elsewhere.[9] With the sample resistance on the order of 0.1 Ω, the four-probe measurement scheme was essential to separate the sample signal from the parasitic resistance of the current leads. The resistance was measured at a direct current of 1 mA. The measurements were made with four different combinations (or channels) of the electrodes as current leads and voltage probes. The resistance measurements in each channel were averaged for the current applied in two opposite directions to cancel the thermal emf. The temperature was measured with a systematic error of 0.5 K (Lakeshore DT-470 sensor).

■ RESULTS AND DISCUSSION

EDXRD Data. Energy-dispersive X-ray diffraction patterns of zirconium and hafnium hydrides in two runs are shown in Figures 2 and 3, respectively. The spectra recorded during compression are given in Figures 2a and 3a, and the decompression spectra are shown in Figures 2b and 3b.

In the EDXRD spectra of all Zr−H runs, we observed a new peak with $d \approx 3.2$ Å emerging at $P \geq 8.2$ GPa. This peak could neither be explained by the predicted bcc-ZrH_3 and hcp-ZrH_3 hydrides nor could it originate from the rhenium gasket (shown in gray in Figure 2b). We observe that the intensity of this peak gradually increased with time, saturating when the pressure reached about 12 GPa. Simultaneously, we observe an appearance of extra peaks, overlapping with the main (101) and (110) peaks from ZrH_2, resulting in an apparent broadening, shift, and intensity change of the peaks. At $P \approx 12$ GPa, the peaks sharpen again, but their positions could no longer be explained by ZrH_2. Such behavior could be explained only by a phase transformation of ZrH_2 to a new yet unknown phase starting at about 8.2 GPa and completing at about 12 GPa. In one run with a larger 2θ scattering angle, we accessed d values down to 1.4 Å and observed six peaks from this new phase (Figure S1 in the Supporting Information). All peaks can be indexed in a body-centered cubic Bravais lattice with $a = 7.84$ Å at 12 GPa. Systematic extinctions are characteristic of the cI16-type structure, previously observed in the Th_4H_{15},[19] NbH_3,[4] and TaH_3[3] hydrides.

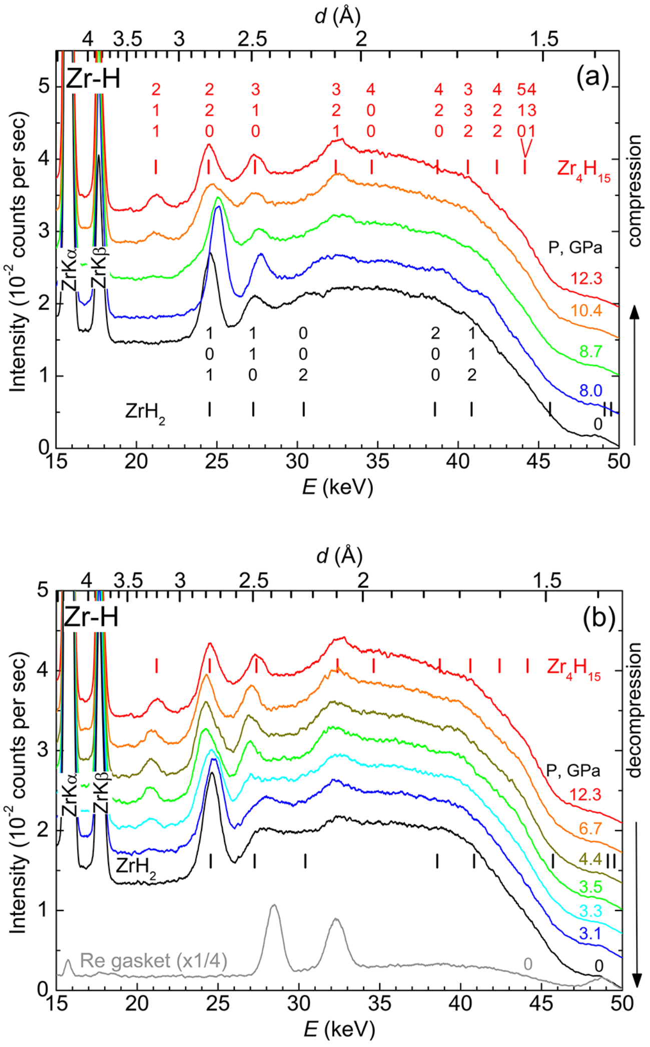

Figure 2. Energy-dispersive X-ray diffraction patterns of Zr hydrides (shifted vertically for clarity) in a hydrogen atmosphere measured during (a) compression and (b) decompression in a DAC in run 3. The peaks at $E < 19$ keV are fluorescence emission lines from zirconium; other peaks are of a diffraction origin. Scattering angle $2\theta = 10.48°$ corresponds to $Ed = 67.9$ keV Å. The black ticks indicate the calculated peak positions for ZrH_2 at ambient pressure (ThH_2 type with $a = 3.52$ Å and $c = 4.46$ Å). The red ticks show the calculated positions of the peaks from new zirconium hydride Zr_4H_{15} at $P = 12.3$ GPa (cI16 type with $a = 7.84$ Å). The gray curve labeled "Re gasket" shows a diffraction pattern from the strongly textured rhenium gasket measured after decompressing the cell to ambient pressure.

The volume effect, accompanying the formation of the novel hydride from ZrH_2, is similar to the volume effect of the ZrH_2 formation from Zr, thus the novel hydride should have a composition close to $ZrH_{\sim 4}$ (i.e., definitely more than H/Zr = 3). A further discussion of volume effects can be found in the next section. Detailed crystal chemistry considerations of possible stoichiometry and hydrogen atom positions in the full crystal structure of a $ThH_{\sim 4}$ hydride with the cI16-type metal sublattice are given in ref 19, where the authors came to the conclusion that it is Th_4H_{15}. These considerations apply equally well to the case of our novel zirconium hydride, justifying its composition to be Zr_4H_{15}.

Experiments with hafnium hydrides have shown that their behavior is nearly identical to that of zirconium hydrides, with the only difference being the formation pressure, which is

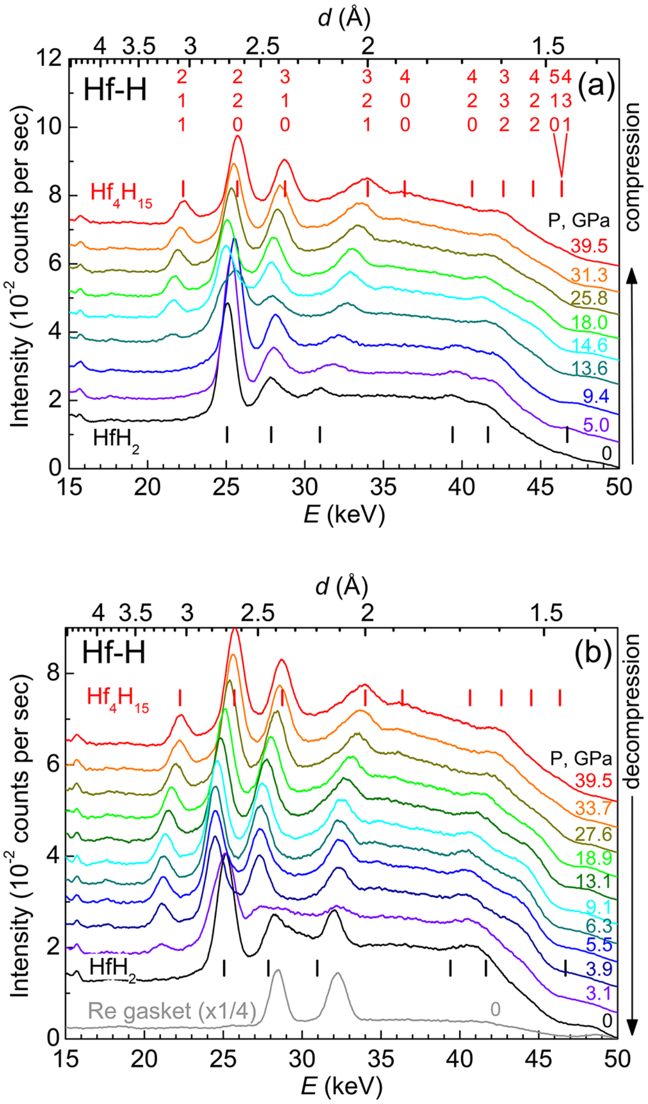

Figure 3. Energy-dispersive X-ray diffraction patterns of Hf hydrides in a hydrogen atmosphere measured in the course of a stepwise pressure (a) increase and (b) decrease in run 4. Scattering angle 2θ = 10.46° corresponds to Ed = 68.0 keV Å. The black ticks indicate the calculated peak positions for HfH_2 at ambient pressure (ThH_2-type lattice with a = 3.45 Å and c = 4.39 Å). The red ticks show the calculated positions of the peaks from new hafnium hydride Hf_4H_{15} at P = 39.5 GPa (cI16-type lattice with a = 7.48 Å). Strong rhenium contamination in the black "0 GPa" spectrum after decompression resulted from the hole collapse after hydrogen escape.

12.4(5) GPa for novel hafnium polyhydride Hf_4H_{15} (Figure 3a).

Until now, among the metal hydrides only Th_4H_{15}, NbH_3, and TaH_3 were found to possess cI16-type metal sublattices. These of NbH_3 and TaH_3 differ from that of Th_4H_{15} only in positional parameter x for metal atoms, resulting in different peak intensity distributions in the second and third peak groups. In the second peak group of Th_4H_{15}, $I(321) > I(400)$, whereas for TaH_3, $I(321) \approx I(400)$ and for NbH_3, $I(321) < I(400)$. In the third peak group of Th_4H_{15}, $I(431) + I(510) > I(332) > I(422)$, whereas for TaH_3, $I(431) + I(510) \approx I(332) \approx I(422)$ and for NbH_3, $I(422) > I(431) + I(510) > I(332)$. In the case of our new zirconium hydride, $I(321) > I(400)$ and $I(431) + I(510) > I(332) > I(422)$ (Figure S1), thus we conclude that the distortion degree of its metal lattice is closer to that of Th_4H_{15} rather than to that of TaH_3 or NbH_3.

New Zr_4H_{15} and Hf_4H_{15} hydrides persist up to the highest pressures reached in our experiments, which were 37 and 40 GPa, respectively. The EDXRD measurements at decompression (Figure 2b) demonstrated that Zr_4H_{15} decomposes back to ZrH_2 at 3.5(3) GPa. For Hf_4H_{15}, the decomposition pressure was 3(1) GPa (Figure 3b).

Volume Effects. To determine the equation of states of new Zr and Hf hydrides, we plot the their $V(P)$ dependencies in Figure 4a,b, respectively, along with the literature data for the compression of pure metals in an inert medium.

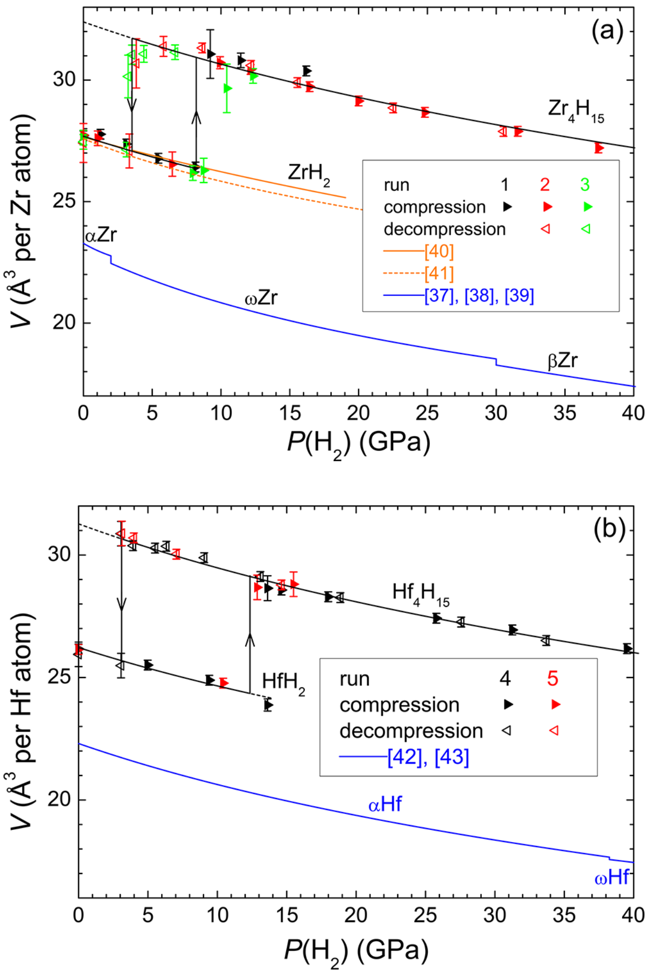

Figure 4. Pressure dependencies of the lattice volumes of (a) Zr and (b) Hf hydrides. The curves show the $V(P)$ dependencies for individual phases, and the vertical lines are drawn at the phase-transition pressures. The equation of state parameters for the black curves are listed in Table 1. The blue curves show the literature data for the compression of α-Zr,[37] ω-Zr,[38] and β-Zr.[39] The literature data for ZrH_2 compression in an inert medium are taken from refs 40 and 41. The $V(P)$ data for Hf were taken from ref 42, and the α ↔ ω equilibrium pressure was taken from ref 43.

The $V(P)$ data points for the two-phase sample states, observed near the formation pressures of new polyhydrides, have the largest volume uncertainty due to severe EDXRD peak overlapping of the MeH_2 and Me_4H_{15} hydrides. Outside of these two-phase regions, the $V(P)$ data points can be fit with the Birch−Murnaghan[44] equation of state

$$P = \frac{3B_0}{2}\left[\left(\frac{V}{V_0}\right)^{-7/3} - \left(\frac{V}{V_0}\right)^{-5/3}\right]\left\{1 + \frac{3}{4}(B_0' - 4)\left[\left(\frac{V}{V_0}\right)^{-2/3} - 1\right]\right\}$$

with fixed bulk modulus pressure derivative $B_0' = 4$, which is a typical value for metals and alloys. For such a fit, we assumed P to be an independent variable and numerically solved the Birch−Murnaghan equation with respect to V for all values of the fitting parameters V_0 and B_0 and experimental P values. The results of the fits are listed in Table 1.

Table 1. Equation of State Parameters for Zr and Hf Hydrides, Resulting from the Fit of the $V(P)$ Data with the Third-Order Birch−Murnaghan Equation of State

substance	V_0, Å^3 per Me atom	B_0, GPa	B_0'	source
α-Zr	23.29(1)	92(3)	4 (fixed)	ref 38
ω-Zr	22.87(10)	90(5)	4 (fixed)	ref 38
	22.7	121	1.69	ref 39
ε-ZrH_2	27.57(2)[a]	150(20)	4 (fixed)	present
	27.59	119(6)	7.7(9)	ref 41
	27.57	174(8)	3.2	ref 40
Zr_4H_{15}	32.4(8)	162(20)	4 (fixed)	present
α-Hf	22.304(25)	112.9(5)	3.29(5)	ref 42
ε-HfH_2	26.03(5)[a]	144(20)	4 (fixed)	present
Hf_4H_{15}	31.3(4)	150(10)	4 (fixed)	present

[a] Results of the refinement of the XRD under ambient conditions from Figure 1.

We observe that the bulk moduli of different Zr and Hf hydrides are practically the same and that the hydrides are significantly less compressible than pure metals. Such behavior is more characteristic of the rare-earth metal hydrides rather than late-transition-metal hydrides, which usually have bulk moduli similar to that of pure metals or are softer.

It should be noted that the composition of all transition-metal hydrides with H/Me > 2, recently synthesized in DACs (except $TaH_{2.2}$, whose composition was measured directly by thermal desorption), was estimated only tentatively by comparing their $V(P)$ dependencies measured by in situ X-ray diffraction with the ab initio calculation predictions. In this way, uncontrollable uncertainties could be introduced, resulting from the limitations of present-day ab initio calculation methods, particularly from the difficulty of taking nonstoichiometricity into account in the calculations.[2,45] All presently available ab initio calculations in the case of Zr−H and Hf−H systems[28−31] failed to reproduce the correct crystal structure of Zr and Hf polyhydrides, and no comparison can be made between theory and experiment at the moment.

An alternative way to estimate the compositions of newly formed hydrides is based on Vegard's law, which assumes that the volumes of different hydrides in a certain metal−hydrogen system, normalized to one metal atom, follow a linear dependence on the H/Me composition. Despite its simplicity, there are two major factors limiting the accuracy of this approach. First, the hydrogen atoms in different interstitials cause a different volume expansion of the host metal lattice,[46] and second, the host metal lattice can change upon hydrogenation.

To verify the applicability of Vegard's law in the case of Zr−H and Hf−H systems, we plotted zero-pressure volumes V_0 for all known phases in these systems as a function of their composition in Figure 5. For comparison, we also present the $V(x)$ data for the Th−H system with the prototypic Th_4H_{15} hydride and for the U−H system[24] in which the U_4H_{15} phase was recently observed but incorrectly identified, as discussed below.

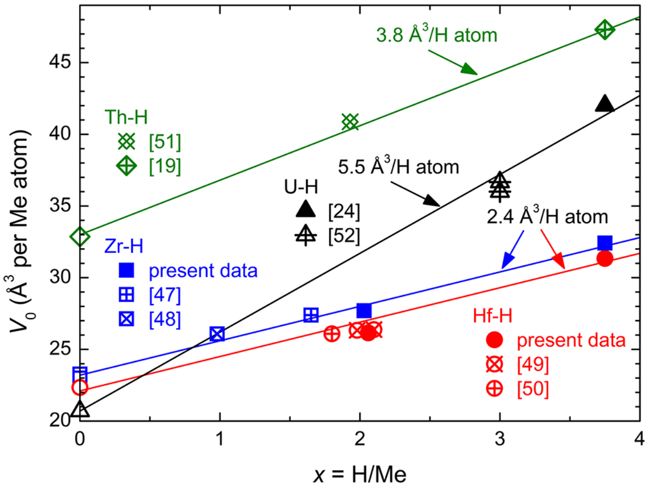

Figure 5. Vegard plots for the Zr−H (blue), Hf−H (red), Th−H (olive), and U−H (black) systems. Present and literature data for hydrides are shown by the filled and crossed symbols, respectively, and the open symbols stand for the literature data for pure elements. The rightmost red and blue symbols correspond to the novel Zr and Hf polyhydrides, assuming their composition to be Me_4H_{15}. The black filled triangle corresponds to an identical phase in the U−H system, observed by Kruglov et al.[24] at nearly ambient pressure after decompressing the UH_x superhydrides, where it was incorrectly identified as *Cmma*(or *Cmcm*)-UH_5. For all points, except those of Zr_4H_{15}, Hf_4H_{15}, and U_4H_{15}, the composition was measured by direct means and its uncertainty is smaller than the symbol size.

The volumes of thorium hydrides, shown by the green symbols in Figure 5, obey Vegard's law with a hydrogen-induced volume expansion of the metal lattice $\beta = (V(\mathrm{MeH}_x) - V(\mathrm{Me}))/x$ of about 3.8 Å^3 per H atom. Such a value of β is rather high compared to the typical values of β = 2−3 Å^3 per H atom for transition and rare earth metal hydrides,[46] which can be associated with the filling of the 5f conduction band in Th hydrides. The applicability of Vegard's law to the Th−H system is surprising in view of the large structural differences between two thorium hydrides.

As shown by the blue and red lines in Figure 5, the volumes of Zr_4H_{15} and Hf_4H_{15} follow Vegard's law with a hydrogen-induced volume expansion of the metal lattice β = 2.4 Å^3 per H atom. Previously, we found that Vegard's law is valid in the Ta−H system with β = 2.4 Å^3 per H atom,[2] thus such a β value should be typical for the hydrides of early transition metals.

In the recent study of the U−H system by Kruglov et al.,[24] a series of new uranium superhydrides were produced under high pressures. After decompressing down to 1 GPa, these hydrides converted to another hydride, identified as *Cmma*(or *Cmcm*)-UH_5. (The corresponding XRD pattern is shown in Figures 4e and S11 in ref 24.) However, the observed XRD pattern could not be satisfactorily explained by these structural models. On the other hand, such an XRD pattern is characteristic of the cI16-type structure with $a \approx 8.75$ Å. The corresponding atomic volume is shown in Figure 5 by a black filled triangle, assuming the composition of this hydride to be U_4H_{15}. The atomic volumes of U_4H_{15} together with that of β-U and well-known α(bcc)-UH_3 and β(A15)-UH_3 trihydrides[52] follow Vegard's law with β = 5.5 Å^3/H atom, as shown by the black line in Figure 5.

Ab initio calculations[24] were unable to reproduce the correct crystal structure of the U_4H_{15} phase, which resulted in a significant composition overestimation for this phase: H/U = 5 instead of the correct value of 3.75. Also, a comparison of the calculated and experimental equations of state of UH_3, which is the only hydride in the U−H system with a reliably determined composition, shows that the calculations dramatically underestimate its volume. We think that a similar situation might have taken place for higher uranium hydrides discovered in ref 24, resulting in their compositions being significantly overestimated. As an alternative way to determine their compositions, we suggest using Vegard's law with β = 5.5 Å^3/H atom.

Electrical Resistance. To determine if the unusual crystal structure of the Th_4H_{15} type gives rise to the superconductivity in novel hydrides, we performed electrical resistance measurements for the Hf−H system in run 6. In this run, HfH_2 was exposed to H_2 at 17 GPa (by H_2 vibron) or at 36 GPa (by diamond Raman line edge) for about 1 week. Hydrogen was deficient, and its vibron could be seen at only one point in the sample. Despite no XRD being measured in this run, from our previous experiments, discussed in the EDXRD Data section, we know that Hf_4H_{15} is formed under such conditions, and we expect that the sample state was a HfH_2 + Hf_4H_{15} mixture. The temperature dependence of the electrical resistance of the sample, measured during warming, is shown in Figure 6. No pressure measurements were made at low temperatures. After warming, the pressure was 23 GPa (by H_2 vibron) or 45 GPa (by diamond Raman edge). We believe that the pressure at low temperature was closer to the final pressure after warming than to the initial pressure before cooling.

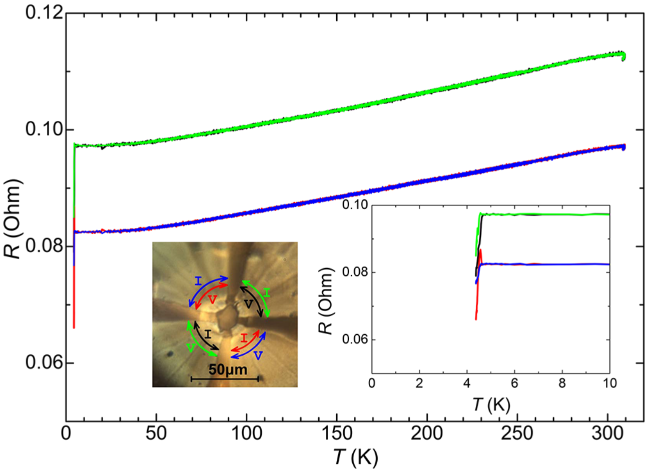

Figure 6. Temperature dependence of resistance in the Hf−H system in run 6, measured with a dc current of 1 mA by a four-probe technique in van der Pauw geometry during warming at $P(H_2)$ = 23 GPa (as measured after warming). (Left inset) Photograph of a sample in combined reflection + transmission illumination and current lead pinout for different channels, represented by four different colors. (Right inset) Magnified view of the $R(T)$ dependence in the low-T region, demonstrating the resistance anomaly at 4.5 K, which can be interpreted as the superconductivity onset in Hf_4H_{15}.

We observed a resistance anomaly at ∼4.5 K, which can be interpreted as a superconductivity onset. Because HfH_2 is not superconductive,[53] this anomaly could be attributed only to Hf_4H_{15}. Regretfully, the present cryogenic equipment did not allow us to cool the sample below 4.4 K to determine if its resistance drops to zero. Further studies are needed to determine the pressure derivative of T_c and the isotope effect. Previously, maximal T_c = 2.23 K in the Hf−H(D) system was observed for primary solid solution $HfD_{0.16}$, obtained by ion implantation.[54]

For Th_4H_{15}, $T_c \approx 8$ K at ambient pressure, and it increases with pressure with an initial slope of 0.0042 K/GPa.[55] Thus, it is reasonable to assume that $T_c(Th_4H_{15}) > T_c(Hf_4H_{15})$, and if the T_c dependence on the metal period number is monotonic, then one can hardly expect higher T_c values in Zr_4H_{15}.

■ CONCLUSIONS

Despite many new superhydrides were predicted by ab initio calculations in recent years, only a limited number of them were observed experimentally. On the other hand, some of the experimentally obtained hydrides were not predicted. In particular, in the Zr−H system all available ab initio calculations[28−31] predicted the formation of ZrH_3 under high hydrogen pressures of a few GPa. Surprisingly, we found that ZrH_3 has no stability field at room temperature, and instead Zr_4H_{15}, which was yet to be predicted, reversibly forms from ZrH_2. The situation is the same for the Hf−H system, in which instead of the predicted HfH_3[29] we observed the formation of Hf_4H_{15}. An analysis of the literature data[24] revealed another polyhydride with this crystal structure type, U_4H_{15}, which was also not predicted.

Our observation that a similar hydride sequence is found in the Zr−H, Hf−H, and Th−H systems provides evidence that the electronic properties of these metals are similar, and as long as its interaction with hydrogen is concerned, thorium behaves as a group IV heavy transition metal. However, the hydrogen-induced volume expansion of thorium is considerably larger than that for Zr and Hf, pointing to the filling of the 5f conduction band in thorium hydrides.

Our electrical resistivity measurements revealed superconductivity in Hf_4H_{15} with $T_c \approx 4.5$ K at 23 GPa, which is not surprising given the analogy between Th_4H_{15} and Hf_4H_{15}. The work is in progress to learn if the mysterious absence of the isotope effect on T_c in Th_4D_{15}[18] also takes place in Hf_4D_{15}.

Assuming that the hydride sequence should be similar for all group IV transition metals, one can expect that titanium should also form a Ti_4H_{15} hydride at sufficiently high hydrogen pressures.

Fortunately, the formation conditions of Zr_4H_{15} are within the reach of modern large-volume high-pressure chambers of the toroid type.[56] This work is in progress to synthesize massive samples of Zr_4H_{15} and Zr_4D_{15} and to recover them to ambient pressure at low temperature. This will allow an accurate investigation of many properties of this hydride by conventional techniques including the determination of its full crystal structure by neutron diffraction.

■ ASSOCIATED CONTENT

Ⓢ Supporting Information

The Supporting Information is available free of charge at https://pubs.acs.org/doi/10.1021/acs.jpcc.9b07918.

Energy-dispersive X-ray diffraction patterns of Zr hydrides (shifted vertically for clarity) in a hydrogen atmosphere measured during compression in a DAC in run 1 (PDF)

AUTHOR INFORMATION

Corresponding Author

*E-mail: kuz@issp.ac.ru.

ORCID

Mikhail A. Kuzovnikov: 0000-0003-4030-4861

Notes

The authors declare no competing financial interest.

ACKNOWLEDGMENTS

The work was partially supported by the Russian Foundation for Basic Research under grant no. 17-02-01142.

REFERENCES

(1) Drozdov, A. P.; Eremets, M. I.; Troyan, I. A.; Ksenofontov, V.; Shylin, S. I. Conventional superconductivity at 203 K at high pressures. *Nature* **2015**, *525*, 73.

(2) Kuzovnikov, M. A.; Tkacz, M.; Meng, H.; Kapustin, D. I.; Kulakov, V. I. High-pressure synthesis of tantalum dihydride. *Phys. Rev. B: Condens. Matter Mater. Phys.* **2017**, *96*, 134120.

(3) Ying, J.; Li, X.; Greenberg, E.; Prakapenka, V. B.; Liu, H.; Struzhkin, V. V. Synthesis and stability of tantalum hydride at high pressures. *Phys. Rev. B: Condens. Matter Mater. Phys.* **2019**, *99*, 224504.

(4) Liu, G.; Besedin, S.; Irodova, A.; Liu, H.; Gao, G.; Eremets, M.; Wang, X.; Ma, Y. Nb-H system at high pressures and temperatures. *Phys. Rev. B: Condens. Matter Mater. Phys.* **2017**, *95*, 104110.

(5) Scheler, T.; Marqués, M.; Konôpková, Z.; Guillaume, C. L.; Howie, R. T.; Gregoryanz, E. High-pressure synthesis and characterization of iridium trihydride. *Phys. Rev. Lett.* **2013**, *111*, 215503.

(6) Pépin, C. M.; Dewaele, A.; Geneste, G.; Loubeyre, P.; Mezouar, M. New iron hydrides under high pressure. *Phys. Rev. Lett.* **2014**, *113*, 265504.

(7) Pépin, C. M.; Geneste, G.; Dewaele, A.; Mezouar, M.; Loubeyre, P. Synthesis of FeH_5: A layered structure with atomic hydrogen slabs. *Science* **2017**, *357*, 382−385.

(8) Geballe, Z. M.; Liu, H.; Mishra, A. K.; Ahart, M.; Somayazulu, M.; Meng, Y.; Baldini, M.; Hemley, R. J. Synthesis and stability of lanthanum superhydrides. *Angew. Chem., Int. Ed.* **2018**, *57*, 688−692.

(9) Drozdov, A. P.; Kong, P. P.; Minkov, V. S.; Besedin, S. P.; Kuzovnikov, M. A.; Mozaffari, S.; Balicas, L.; Balakirev, F.; Graf, D.; Prakapenka, V. B.; et al. Superconductivity at 250 K in lanthanum hydride under high pressures. *Nature* **2019**, *569*, 528−531.

(10) Somayazulu, M.; Ahart, M.; Mishra, A. K.; Geballe, Z. M.; Baldini, M.; Meng, Y.; Struzhkin, V. V.; Hemley, R. J. Evidence for superconductivity above 260 K in lanthanum superhydride at megabar pressures. *Phys. Rev. Lett.* **2019**, *122*, 027001.

(11) Li, X.; Huang, X.; Duan, D.; Pickard, C. J.; Zhou, D.; Xie, H.; Zhuang, Q.; Huang, Y.; Zhou, Q.; Liu, B.; et al. Polyhydride CeH_9 with an atomic-like hydrogen clathrate structure. *Nat. Commun.* **2019**, *10*, 3461.

(12) Salke, N. P.; Esfahani, M. M. D.; Zhang, Y.; Kruglov, I. A.; Zhou, J.; Wang, Y.; Greenberg, E.; Prakapenka, V. B.; Oganov, A. R.; Lin, J.-F. Synthesis of clathrate cerium superhydride CeH_9 at 80−100 GPa with atomic hydrogen sublattice. *Nat. Commun.* **2019**, *10*, 4453.

(13) Zhou, D.; Semenok, D. V.; Duan, D.; Xie, H.; Huang, X.; Chen, W.; Li, X.; Liu, B.; Oganov, A. R.; Cui, T. *Superconducting praseodymium superhydrides*. https://arxiv.org/abs/1904.06643 (accessed Aug 15, 2019).

(14) Peña-Alvarez, M.; Binns, J.; Hermann, A.; Kelsall, L. C.; Dalladay-Simpson, P.; Gregoryanz, E.; Howie, R. T. Praseodymium polyhydrides synthesized at high temperatures and pressures. *Phys. Rev. B: Condens. Matter Mater. Phys.* **2019**, *100*, 184109.

(15) Zhou, D.; Semenok, D. V.; Xie, H.; Kartsev, A. I.; Kvashnin, A. G.; Huang, X.; Duan, D.; Oganov, A. R.; Cui, T. *High-pressure synthesis of magnetic neodymium polyhydrides*. https://arxiv.org/abs/1908.08304 (accessed Nov 13, 2019).

(16) Troyan, I. A.; Semenok, D. V.; Kvashnin, A. G.; Ivanova, A. G.; Prakapenka, V. B.; Greenberg, E.; Gavriliuk, A. G.; Lyubutin, I. S.; Struzhkin, V. V.; Oganov, A. R. *Synthesis and superconductivity of yttrium hexahydride Im-3m-YH_6*. https://arxiv.org/abs/1908.01534 (accessed Nov 13, 2019).

(17) Kong, P. P.; Minkov, V. S.; Kuzovnikov, M. A.; Besedin, S. P.; Drozdov, A. P.; Mozaffari, S.; Balicas, L.; Balakirev, F. F.; Prakapenka, V. B.; Greenberg, E. et al. *Superconductivity up to 243 K in yttrium hydrides under high pressure*. https://arxiv.org/abs/1909.10482 (accessed Nov 13, 2019).

(18) Satterthwaite, C. B.; Toepke, I. L. Superconductivity of hydrides and deuterides of Thorium. *Phys. Rev. Lett.* **1970**, *25* (11), 741−743.

(19) Zachariasen, W. H. Crystal chemical studies of the 5f-series of elements. XIX. The crystal structure of the higher thorium hydride, Th_4H_{15}. *Acta Crystallogr.* **1953**, *6*, 393−395.

(20) Mueller, M. H.; Beyerlein, R. A.; Jorgensen, J. D.; Brun, T. O.; Satterthwaite, C. B.; Caton, R. Structure of Th_4D_{15} from measurements at the Argonne ZING-P pulsed neutron source. *J. Appl. Crystallogr.* **1977**, *10*, 79−83.

(21) Hanfland, M.; Syassen, K.; Christensen, N. E.; Novikov, D. L. New high-pressure phases of lithium. *Nature* **2000**, *408*, 174−178.

(22) McMahon, M. I.; Gregoryanz, E.; Lundegaard, L. F.; Loa, I.; Guillaume, C.; Nelmes, R. J.; Kleppe, A. K.; Amboage, M. Structure of sodium above 100 GPa by single-crystal x-ray diffraction. *Proc. Natl. Acad. Sci. U. S. A.* **2007**, *104* (44), 17297−17299.

(23) Sugimoto, T.; Akahama, Y.; Fujihisa, H.; Ozawa, Y.; Fukui, H.; Hirao, N.; Ohishi, Y. Identification of superlattice structure cI16 in the P-VI phase of phosphorus at 340 GPa and room temperature via x-ray diffraction. *Phys. Rev. B: Condens. Matter Mater. Phys.* **2012**, *86*, 024109.

(24) Kruglov, I. A.; Kvashnin, A. G.; Goncharov, A. F.; Oganov, A. R.; Lobanov, S. S.; Holtgrewe, N.; Jiang, S.; Prakapenka, V. B.; Greenberg, E.; Yanilkin, A. V. Uranium polyhydrides at moderate pressures: Prediction, synthesis, and expected superconductivity. *Sci. Adv.* **2018**, *4*, No. eaat9776.

(25) Semenok, D. V.; Kvashnin, A. G.; Ivanova, A. G.; Svitlyk, V.; Fominski, V. Yu.; Sadakov, A. V.; Sobolevskiy, O. A.; Pudalov, V. M.; Troyan, I. A.; Oganov, A. R. Superconductivity at 161 K in thorium hydride ThH_{10}: Synthesis and properties. *Mater. Today* **2019**, *xx*, xxxx.

(26) Manchester, F. D.; San-Martin, A. *Phase Diagrams of Binary Hydrogen Alloys*; ASM International: Materials Park, 2000.

(27) Bashkin, I. O.; Malyshev, V. Yu.; Ponyatovsky, E. G. Phase transformations in the Ti—H and Zr—H systems at high and atmospheric pressures. *Z. Phys. Chem.* **1993**, *179*, 289−99.

(28) Han, Z.-Z.; Lu, Y.; Wang, W.; Hou, Z.-L.; Shao, X.-H. The novel structure and superconductivity of zirconium hydride. *Comput. Mater. Sci.* **2017**, *134*, 38−41.

(29) Bourgeois, N.; Crivello, J.-C.; Cenedese, P.; Joubert, J.-M. Systematic first-principles study of binary metal hydrides. *ACS Comb. Sci.* **2017**, *19*, 513−523.

(30) Li, X.-F.; Hu, Z.-Y.; Huang, B. Phase diagram and superconductivity of compressed zirconium hydrides. *Phys. Chem. Chem. Phys.* **2017**, *19*, 3538−3543.

(31) Abe, K. High-pressure properties of dense metallic zirconium hydrides studied by ab initio calculations. *Phys. Rev. B: Condens. Matter Mater. Phys.* **2018**, *98*, 134103.

(32) Tkacz, M. Novel High-pressure technique for loading diamond anvil cell with hydrogen. *Polym. J. Chem.* **1995**, *69*, 1205−1209.

(33) Mao, H. K.; Xu, J.; Bell, P. M. Calibration of the ruby pressure gauge to 800 kbar under quasi-hydrostatic conditions. *J. Geophys. Res.* **1986**, *91* (5), 4673−4676.

(34) Tkacz, M.; Majchrzak, S.; Baranowski, B. High pressure X-ray diffraction study of copper hydride at room temperature. *High Pressure Res.* **1990**, *6* (2), 85−90.

(35) Akahama, Y.; Kawamura, H. Pressure calibration of diamond anvil Raman gauge to 310 GPa. *J. Appl. Phys.* **2006**, *100*, 043516.

(36) Sharma, S. K.; Mao, H. K.; Bell, P. M. Raman measurements of hydrogen in the pressure range 0.2−630 kbar at room temperature. *Phys. Rev. Lett.* **1980**, *44*, 886−888.

(37) Olinger, B.; Jamieson, J. C. Zirconium: phases and compressibility to 120 kilobars. *High Temp.-High Pres.* **1973**, *5*, 123−131.

(38) Zhao, Y.; Zhang, J.; Pantea, C.; Qian, J.; Daemen, L. L.; Rigg, P. A.; Hixson, R. S.; Gray, G. T.; Yang, Y.; Wang, L.; et al. Thermal equations of state of the α, β, and ω phases of zirconium. *Phys. Rev. B: Condens. Matter Mater. Phys.* **2005**, *71*, 184119.

(39) Akahama, Y.; Kobayashi, M.; Kawamura, H. High-Pressure X-Ray diffraction study on electronics-d transition in zirconium. *J. Phys. Soc. Jpn.* **1991**, *60* (10), 3211−3214.

(40) Lityagina, L. M.; Dyuzheva, T. I. Isothermal compression study of 3d and 4d transition metal dihydrides II: Compression of $ZrH_{1.99}$ up to 18 GPa. *J. Alloys Compd.* **1992**, *179*, 73−76.

(41) Huang, X.; Duan, D.; Li, F.; Huang, Y.; Wang, L.; Liu, Y.; Bao, K.; Zhou, Q.; Liu, B.; Cui, T. Structural stability and compressive behavior of ZrH_2 under hydrostatic pressure and nonhydrostatic pressure. *RSC Adv.* **2014**, *4*, 46780.

(42) Hrubiak, R.; Drozd, V.; Karbasi, A.; Saxena, S. K. High P-T phase transitions and P-V-T equation of state of hafnium. *J. Appl. Phys.* **2012**, *111*, 112612.

(43) Xia, H.; Parthasarathy, G.; Luo, H.; Vohra, Y. K.; Ruoff, A. L. Crystal structures of group IVa metals at ultrahigh pressures. *Phys. Rev. B: Condens. Matter Mater. Phys.* **1990**, *42*, 6736−6738.

(44) Birch, F. Finite Elastic Strain of Cubic Crystals. *Phys. Rev.* **1947**, *71* (11), 809−824.

(45) Kuzovnikov, M. A.; Meng, H.; Tkacz, M. Nonstoichiometric molybdenum hydride. *J. Alloys Compd.* **2017**, *694*, 51−54.

(46) Fukai, Y. *The Metal-Hydrogen System*, 2nd ed.; Springer-Verlag: Berlin, 2005; pp 104−113.

(47) Bowman, R. C., Jr.; Craft, B. D.; Cantrell, J. S.; Venturini, E. L. Effects of thermal treatments on the lattice properties and electronic structure of ZrH_x. *Phys. Rev. B: Condens. Matter Mater. Phys.* **1985**, *31*, 5604−5615.

(48) Kolesnikov, A. I.; Balagurov, A. M.; Bashkin, I. O.; Belushkin, A. V.; Ponyatovsky, E. G.; Prager, M. Neutron scattering studies of ordered γ−ZrD. *J. Phys.: Condens. Matter* **1994**, *6*, 8977−8988.

(49) Sidhu, S. S. The effect on metal−metal bonds of increased concentration of hydrogen in hafnium dihydride. *Acta Crystallogr.* **1954**, *7*, 447−449.

(50) Sidhu, S. S.; McGuire, J. C. An x-ray diffraction study of the hafnium-hydrogen system. *J. Appl. Phys.* **1952**, *23*, 1257.

(51) Korst, W. L. The lattice constants of thorium dihydride. *Acta Crystallogr.* **1962**, *15*, 287−288.

(52) Mulford, R. N. R.; Ellinger, F. H.; Zachariasen, W. H. A new form of uranium hydride. *J. Am. Chem. Soc.* **1954**, *76*, 297−298.

(53) Bashkin, I. O.; Antonov, V. E.; Ponyatovsky, E. G. *Studies of High Temperature Superconductors;* Nova Science Publishers: New York, 2003; Vol. *45*, pp 171−241.

(54) Meyer, J. D.; Stritzker, B. H and D implantation transforms Ti, Zr and Hf into good superconductors. *Nucl. Instrum. Methods* **1981**, *182−183*, 933−936.

(55) Dietrich, M.; Gey, W.; Rietschel, H.; Satterthwaite, C. B. Pressure dependence of the superconducting transition temperature of Th_4H_{15}. *Solid State Commun.* **1974**, *15*, 941−943.

(56) Khvostantsev, L. G.; Slesarev, V. N.; Brazhkin, V. V. Toroid type high-pressure device: history and prospects. *High Pressure Res.* **2004**, *24* (3), 371−383.

DOI: 10.1021/acs.jpcc.9b07918
J. Phys. Chem. C 2019, 123, 30059−30066